PROCEEDINGS OF SCIENCE

Energy dependence of μ^- transfer rate to Oxygen

D. Bakalov,[a,*] **M.N. Stoilov**[a] **and P. Danev**[a]

[a] *Institute for Nuclear Research and Nuclear Energy - Bulgarian Academy of Sciences, 72 Tzarigradsko Chaussée, Sofia, Bulgaria*

E-mail: bakal10@abv.bg

The exotic atom of muonic hydrogen $p\mu$ has a relatively long lifetime allowing for precise measurements of its spectra. The hyperfine splitting of its ground-state $\Delta E^{\rm hfs} \sim 0.182$ eV is in the infra-red optical range that makes it convenient to be studied with laser spectroscopy. Several experiments for the determination of the proton Zemach radius from measurements of $\Delta E^{\rm hfs}$, are currently underway. One of them is the FAMU experiment, aiming to determine the Zemach radius of the proton by studying the time distribution of the characteristic X-rays signaling the laser-stimulated spin-flip of the $p\mu$ atoms. As the accurate knowledge of the collision energy dependence of the muon transfer rate from the ground-state of $p\mu$ to oxygen, $\lambda_{\rm pO}(E)$, is crucial for the efficiency of the FAMU method, we use the available data from recent measurements of the muon transfer rate at temperatures in the range 70 K$<T<$336 K in fully thermalized gas to obtain reliable estimates of $\lambda_{\rm pO}(E)$ by fitting the experimental data with various trial functions. The advantages and disadvantages of each type of trial functions are discussed in detail.

11th International Conference of the Balkan Physical Union (BPU11),
28 August - 1 September 2022
Belgrade, Serbia

*Speaker

PoS(BPU11)065

1. Introduction

The light exotic atoms posses unique characteristics allowing them to be used as alternative to the standard atoms in studying the basic properties of matter [1–4]. The most precise determinations of the proton charge radius were carried out by spectroscopy measurements of muonic atoms [1, 5]. That is how the so-called "proton radius puzzle" arose when R. Pohl *et al.*, studied the Lamb shift in muonic hydrogen and discovered that the proton radius they measured was smaller than previously thought [1]. In the following years new experiments investigated this discrepancy [6, 7]. Although this question is now almost closed, the uncertainties in other fundamental characteristics, such as the proton Zemach radius remain an open problem.

The FAMU project is dedicated to determine the proton Zemach radius, a convolution of the magnetic dipole and electric charge distribution in the proton [4]. It will be extracted by measurements of the resonance frequency of the singlet to triplet transition in the ground state of $p\mu$ stimulated by a laser, tunable around the resonance frequency $\Delta E^{\rm hfs}/h \sim 44$ THz [4, 8]. This transition will be recognized by the response of the time distribution of the characteristic muonic oxygen X-rays, which in turn is sensitive to the kinetic energy dependence of the rate of muon transfer from muonic hydrogen to muonic oxgen [9–11], thus it is imperative to have an accurate knowledge of the energy dependence of the muon transfer reaction, $\lambda_{\rm pO}(E)$. In this work, we investigate several functional dependencies $\lambda_{\rm pO}(E)$, obtained by fitting experimental data to different test functions. The initial data points are taken from the recent FAMU measurements of the muon transfer rate's temperature dependence for several temperatures in the range 70 K$<T<$336 K [12]. Our computations show that, when the fitting functions are constrained by a few physical requirements, the resulting functions describe the behavior of $\lambda_{\rm pO}(E)$ quite accurately.

The work is organized as follows. In Sec. 2, a brief summary of the FAMU experiment is given. The method used to extract the Zemach radius from mesurements of the hyperfine splitting in its ground state is explained in Sec. 2.1. Next, we present the results from the latest FAMU measurements of the temperature dependence of the transfer rate of muons, used as input data latter in this paper 2.2. In Sec. 3.1 several fits when we do not place any requirements on the type of functions are studied. Next, in Sec. 3.2 various constrained fitting functions for $\lambda_{\rm pO}(E)$ are reviewed and their advantages and disadvantages are assessed. The results from this work are summarized in Sec. 4.

2. The FAMU experiment

2.1 Summary of the experimental method

The FAMU project is dedicated to determine with high accuracy the proton Zemach radius and in this way to find an independent solution to the "proton size puzzle". The method consists of a series of steps as shown on Fig. 1:

1. The $p\mu$'s in 1s($\uparrow\downarrow$) state propagate in a H_2 and O_2 gas mixture.
2. Part of the $p\mu$'s are excited to the 1s($\uparrow\uparrow$) state with laser pulse.
3. In collisions with H_2 the $p\mu$'s are de-excited back to ($\uparrow\downarrow$) state. These atoms carry away nearly 2/3 of the released energy $E^{\rm hfs}(\sim 0.12$ eV) as additional kinetic energy.

4. In collisions of $p\mu$ with O_2 the muon is transferred to an excited state of muonic oxygen μO^*. The rate of muon transfer to oxygen from accelerated $p\mu$'s exceeds the rate from thermal $p\mu$'s.

5. The muon transfer to oxygen is signaled by the emission of characteristic X-rays during relaxation of μO^*.

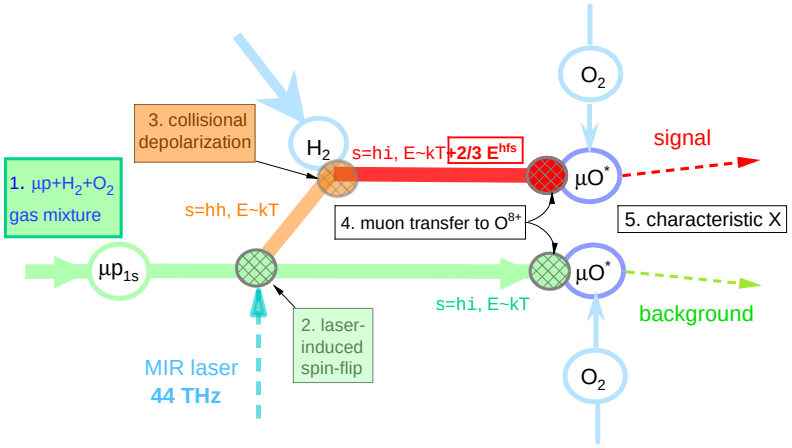

Figure 1: (Color online) The method used in FAMU experiment for determination of the proton Zemach radius by studying the transfer rate of μ^- from hydrogen to oxygen in the presence and absence of a laser field with resonant for the ground state otho-para transition frequency.

The experimental observable is the time distribution characteristic of X-rays (see Fig. 2). The signal is the time distribution difference in the X-rays with and without laser pulse. The more spin-flipped μp's, the stronger the signal. It reaches maximum at laser frequency in resonance with the hyperfine splitting ΔE^{hfs}. The fast muon transfer from accelerated μp perturbs the exponential background from thermal μp's.

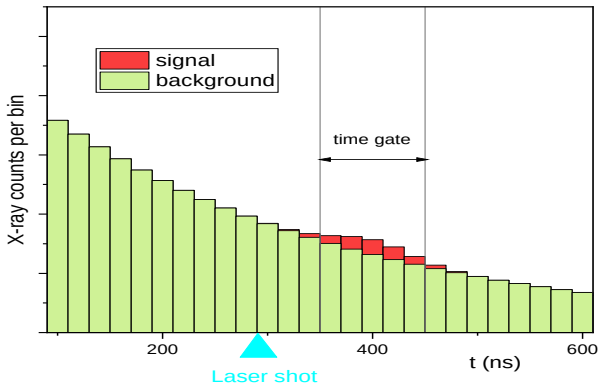

Figure 2: (Color online) Time distribution of the characteristic X-rays from the muonic oxygen. The signal represents an excess in X-rays indicating the increase in the characteristic radiation when the infrared laser is tuned to the resonance frequency E^{hfs}.

It can be seen that the efficiency of the method is determined by the collision energy dependence

$\lambda_{pO}(E)$ of the rate of muon transfer $(p\mu)_{1s} + O \to (O\mu)^* + p$. There are indications of a sharp raise of $\lambda_{pO}(E)$ at thermal and near epithermal energies in hydrogen-oxygen admixture [9–11]. However, more accurate quantitative experimental verification is needed.

2.2 Temperature dependence of the muon transfer rate

Recently, the FAMU collaboration measured the temperature dependence $\Lambda_{pO}(T)$ of the muon transfer rate for several temperatures in the range 70 K<T<336 K in fully thermalized gas [12]. The results for $\Lambda_{pO}(T)$, with the experimental uncertainties $\delta\Lambda$ are given in Table 1.

However, what we actually need is the transition rate as a function of μp's kinetic energy $\lambda_{pO}(\mathbf{E})$. Let $f(E;T)$ is the energy distribution of μp. In thermal equilibrium this is the Maxwell-Boltzmann distribution

$$f(E;T) = f_{MB}(E;T) = \frac{2}{\sqrt{\pi}(kT)^{3/2}}\sqrt{E}\exp(-E/kT). \tag{1}$$

Then, the temperature dependence $\Lambda_{pO}(T)$ of the rate of muon transfer can be written as:

$$\Lambda_{pO}(T) = \int dE\, \lambda_{pO}(E)\, f(E;T) \tag{2}$$

Since, we know the values of $\Lambda_{pO}(T)$ for only few discrete points, the inverse Laplace transform is

k	1	2	3	4	5	6	7	8	9	10
T_k	70	80	104	153	201	240	272	300	323	336
Λ_k	2.67	2.96	3.07	5.20	6.48	8.03	8.18	8.79	8.88	9.37
$\delta\Lambda_k$	0.51	0.38	0.30	0.34	0.35	0.38	0.41	0.43	0.91	1.07

Table 1: Temperature dependence of the muon transfer rate from hydrogen to oxygen $\Lambda_{pO}(T)$ for 10 temperatures in the range 70 K<T<336 K in fully thermalized gas measured by the FAMU collaboration [12]. The values shown are normalized to liquid hydrogen, in units 10^{10} s^{-1}.

inapplicable for deriving the energy dependence of the muon transfer rate $\lambda_{pO}(E)$. Our approach in this work will be to probe various trial functions $\lambda_{pO}(E;\{p\})$, for which $\Lambda_{pO}(T;\{p\})$, calculated with Eq. (2) gives best fit of the data.

3. Searching for functional dependence of the transfer rate

3.1 Fits with unconstrained test functions

In this chapter we fit the experimental data for $\Lambda_{pO}(T)$ to few-parameter functions and estimate how well the corresponding $\lambda_{pO}(E)$ describe the behavior of muon transfer rate in the energy range of interest for the FAMU experiment. Here, we will not constrain the fitting expressions and we will investigate their goodness of fit. Six test functions are studied:

$$\begin{aligned} &(a) \quad a_0 + a_1\sqrt{E}; && (b) \quad a_0 + a_1 E; \\ &(c) \quad a_0 E + a_1 E^3; && (d) \quad a_0 + a_1 E^2 + a_2 E^3; \\ &(e) \quad (a_0 + a_1 E + a_2 E^2)e^{-E/e_1}; && (f) \quad a_0 + a_1 E + a_2 E^2. \end{aligned} \tag{3}$$

From Fig. 3(left), in can be seen that all expressions fit the data very well. However, outside the region for which data points are available, the fits diverge.Some of the curves show unphysical negative values for the energy dependence of the muon transfer. The above results show that the correct behavior of $\lambda_{pO}(E;\{p\})$ can not be determined unambiguously with only ten data-points and standard fitting procedure. As a conclusion: the unconstrained test functions reproduce the data well (low chi-squared χ^2), but diverge outside the range of investigated temperatures, and lead to unphysical values and wrong asymptotics.

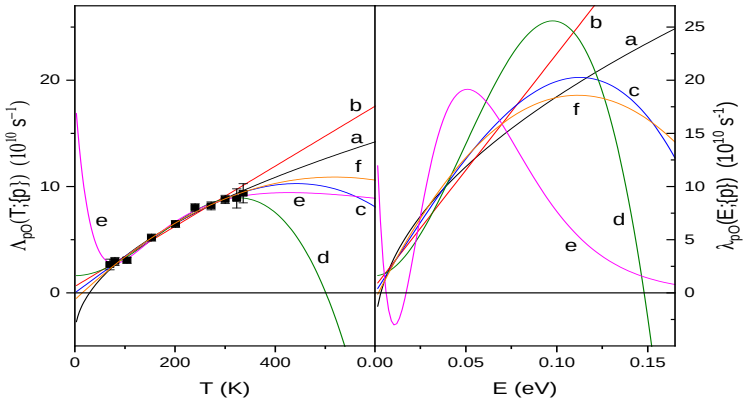

Figure 3: (Color online) The results of fitting the FAMU data for $\Lambda_{pO}(T)$ with the functions given by Eq. (3)(left). On the right picture are presented the functions for $\lambda_{pO}(E;\{p\})$, corresponding to $\Lambda_{pO}(T)$ with the same letter.

3.2 Constrained experimental data fits

The above-mentioned issue could be solved if we impose certain physical constraints on the fitting functions:

C1 - Non-negativity: $\lambda(E;\{p\}) \geq 0$ for all $E \geq 0$. Out of the examples on Fig. 3 this excludes cases (c), (d), (e), and (f).

C2 - Large E asymptotics: $d\lambda(E;\{p\})/dE \leq 0$ for $E > \varepsilon_\mu = m_\mu c^2\alpha^2 \sim 5$ keV.

C3 - Agreement with Wigner threshold law: $\lambda_0 = \lambda(0;\{p\}) > 0$,
$0 \leq d\lambda(E;\{p\})/dE \ll \lambda_0/E_0$ for $E < E_0$, $E_0 \sim 10^{-3}$ eV

C4 - Stability: No qualitative changes if fitting data subsets.

We investigate a few types of functions, from simple to more complicated ones, and for each we analyze their advantages and disadvantages in regarding the reliability of resulting expression for $\lambda_{pO}(E)$.

3.2.1 Truncated polynomials

The best fit with the polynomial function

$$\lambda(E)=\max(p_0+p_1E+p_2E^2,0) \tag{4}$$

is shown on Fig. 4 (Left). On the right picture is presented the corresponding function $\lambda_{\mathrm{pO}}(E)$ computed by means of Eq. (2). The shadowed area is the mean prediction band (MPB) for 95% confidence level.

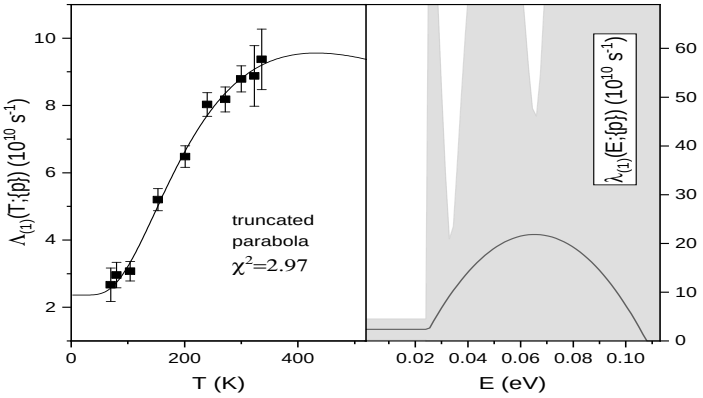

Figure 4: (Left) Fit of the experimental data for $\Lambda_{\mathrm{pO}}(T)$ with the truncated polynomial given in Eq. (4). The experimental uncertainties are presented too. (Right) The corresponding curve for $\lambda_{\mathrm{pO}}(E)$ with its confidence band shown in gray.

This function satisfies conditions C1 and C2. However, the confidence band is very wide and this fit cannot give good predictions for the energy dependence of the muon transfer rate from hydrogen to oxygen.

3.2.2 Cubic spline test functions

We have investigated two types of cubic splines. In the first case the experimental data is fitted by 3-node splines. As seen on Fig. 5, the MPB for 95% confidence level for both cases is at fairly acceptable level. The functions $\lambda(E)$ are positive in the shown energy interval, and condition C2 is satisfied too.

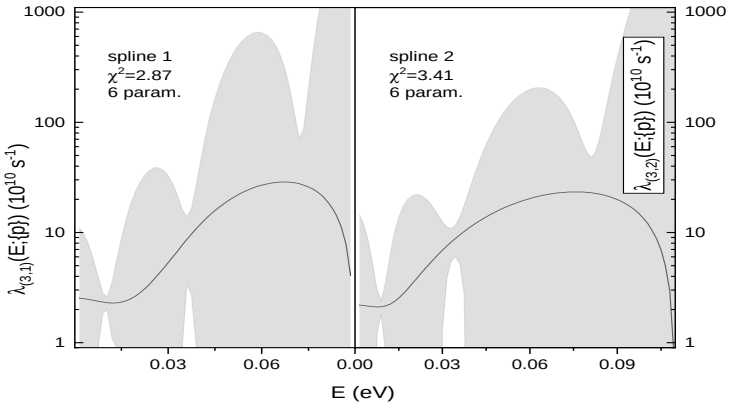

Figure 5: Two optimal fits of the available data for the temperature dependence of the muon transfer rate with 3-node cubic spline.

We made fits with 5-node cubic spline too. However, due to the low number of data points and relatively high number of fitting parameters, the results are not so promising. The confidence

bands are narrower, but the energy dependence of the μ^- transfer rate becomes negative at some point < 0.15 EV. One of the optimal examples is given on Fig. 6.

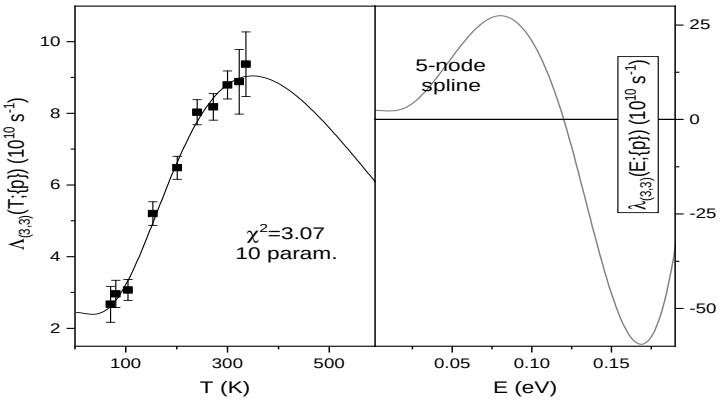

Figure 6: Optimal fit of the temperature dependence of the muon transfer rate with 5-node cubic spline. The functions $\Lambda_{\mathrm{pO}}(T)$ and $\lambda_{\mathrm{pO}}(E;\{p\})$ are shown on the left and right picture respectively.

From the investigated examples for piece-wise test functions, few conclusions could be made. They fit the experimental data ($\Lambda_{\mathrm{pO}}(T)$) quite well, and selected examples satisfy the conditions from the beginning of the section. However, the confidence bands are unacceptably wide. In the next section, we present the results of more complex flexible few-parameter smooth test functions.

3.2.3 C^∞ test functions

Here we will show the best results of fitting the experimental data with two types of functions, which we can generally write as:
Type 1: Gaussian-like behavior at large E

$$\lambda_{(5)}(E;\{p\}) = \Big(\sum_{k=1}^{N} p_k E^{\alpha_k}\Big)\exp(-(E-p_{N+1})^2/p_{N+2}^2) + p_{N+3}, \tag{5}$$

Type 2: Exponential behavior at large E

$$\lambda_{(6)}(E;\{p\}) = \Big(\sum_{k=1}^{N} p_k E^{\alpha_k}\Big)\exp(-E/p_{N+1}) + p_{N+2}. \tag{6}$$

The parameters α_k are preselected, and some could be equal to zero. N is positive integer. The parameters $p_1, .., p_{N+3}$ are found by the fitting procedure.

The simplest case of the Gaussian-like type functions Eq. (7) is when $N = 1$ and $\alpha_1 = 0$. It is quite successful as can be verified from Fig. 7. All criteria C1, C2, C3, and to some extent C4, are satisfied. Chi-squared per degrees of freedom is relatively good too.

A better fit is achiever for $N = 2$, when the following 4-parameter modification is used:

$$\lambda_{5*}(E;\{p\}) = \lambda_5(E;\{p\}) - d\lambda_5(0;\{p\})/dE - d^2\lambda_5(0;\{p\})/dE^2 \tag{7}$$

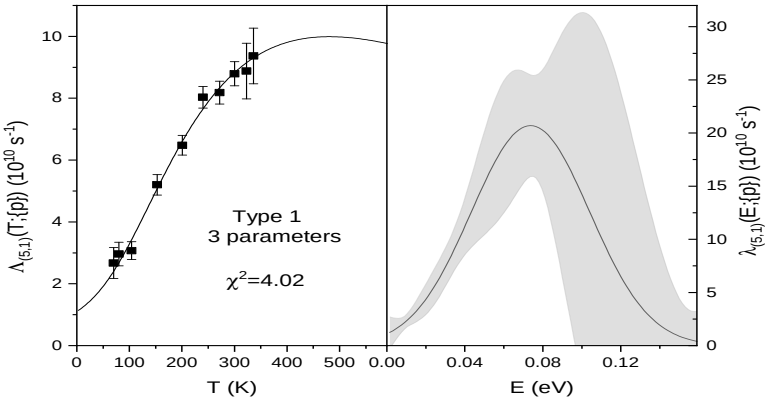

Figure 7: A simple fit with Gaussian-like test function given by Eq. (5). Regardless of the small number of parameters, the error band at 95% confidence level (on the right picture) is relatively low.

Its main advantage is that it better complies with Wigner law (C3). So, all four physical requirements are satisfied. Two of the most promising fits of this type are shown on Fig. 8. The blue and red curves correspond to $\Lambda_{(5*,1)}(T)$ and $\Lambda_{(5*,2)}(T)$ on the left picture and $\lambda_{(5*,1)}(E)$ and $\lambda_{(5*,2)}(E)$ - on the right one respectively. Although their parameters α_k and p_k are quite different, both have similar behavior as function of temperature and of energy. The confidence band is narrow for $E < 75$ meV, and in acceptable level up to = 100 meV.

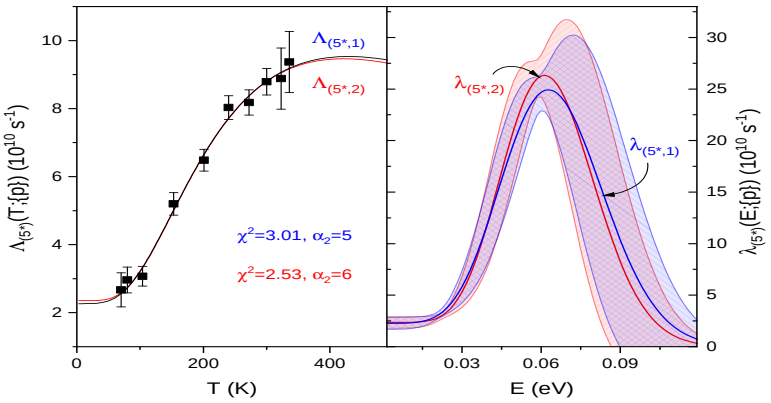

Figure 8: (Color online) The best fits obtained with modification (7) of the Gaussian-like test function given by Eq. (5). Both blue and red lines on the left (representing $\Lambda_{5*}(T)$) and the right ($\lambda_{5*}(E)$) pictures are obtained for different parameters α_2. The shadowed areas (light blue and light red) on the right figure correspond to the respective transition rates' confidence bands.

The best fits with test functions having exponential behavior for large energy Eq. (6), shown in Fig. 9, satisfy all criteria C1-C4, have narrow uncertainties (better for low energies), and low $\chi^2/n.d.f$. They were obtained with N=2, $\alpha_1 = 0$ and the following three-parameter expression:

$$\lambda_{6*}(E;\{p\}) = \lambda_6(E;\{p\}) - d\lambda_6(0;\{p\})/dE - d^2\lambda_6(0;\{p\})/dE^2. \tag{8}$$

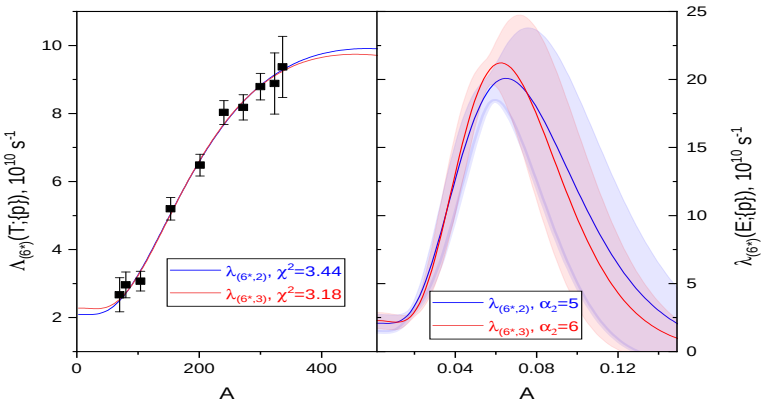

Figure 9: (Color online) The best fits obtained with modification (8) of the Gauss test function given by Eq. (6). Both blue and red lines on the left (representing $\Lambda_{6*}(T)$) and the right ($\lambda_{6*}(E)$) pictures are obtained with different fitting parameters. The shadowed areas (light blue and light red) on the right figure correspond to the respective transition rates' uncertainty bands.

The fits with flexible few-parameter smooth test functions Eqs. (5) and (6) presented on Figs. 8 and 9, describe well the experimental data for the temperature dependence of the muon transfer rate. Those fitting functions have low confidence bands and agree very well with the restrictions given at the beginning of the section. It is important to note that all of them show similar behavior in the whole energy range of interest, although they are obtained with different functions and function's parameters.

3.2.4 Best fit

In the preceding section, we investigated various few-parameter trial function types that lead to fits of the experimental data of competitive quality. On Fig. 10 are shown the optimized trial functions (qubic spline, Type 1 of Eq. (5), Type 2 of Eq. (6) and the modifications of Eqs. (7), (8)), which correspond to the optimal fits of the $\Lambda_{\mathrm{pO}}(T)$ data, have the lowest χ^2 and satisfy conditions C1-C4. We assume that the envelope of the set of selected 7 curves delimits the model uncertainty band of the experimentally determined energy dependence of the rate of muon transfer to oxygen; it is represented by the shadowed area on Fig. 10. We define as best fit to the muon transfer energy dependence $\lambda_{\mathrm{best}}(E)$ the median of the model uncertainty band; it is represented by the thick line on Fig. 10. For energies below 80 meV the model uncertainty does not exceed 20%.

4. Summary and conclusion

We have shown that the problem of extracting the energy dependence of the muon transfer rate from hydrogen to oxygen from the sparse data available does not have a unique solution. By imposing a few physically motivated constraints on the fitting functions, the uncertainty of the results was reduced to an acceptable level. We have found several expressions that fit the data well and could be used in further studies on the topic. Adding additional experimental data will further restrict the fitting parameter space and will increase the reliability of the derived fitting expressions.

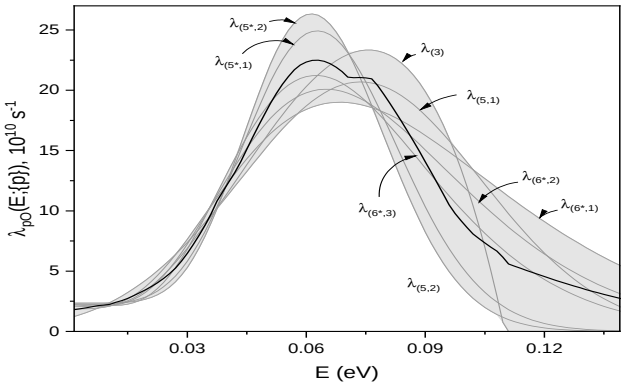

Figure 10: A combination of the best fits with functions considered in this work: λ_3 corresponds to qubic spline, $\lambda_{5,1}$ and $\lambda_{5,2}$ - to Eq. (5), $\lambda_{5^*,1}$ and $\lambda_{5^*,2}$ - to Eq. (7), and $\lambda_{6^*,1}$, $\lambda_{6^*,2}$, $\lambda_{6^*,3}$ - to Eq. (8). The model's uncertainty is represented by the shadowed area and is given by the envelope of the seven fits. The thick line is the envelope's median and corresponds to the best fit.

The results presented here reveal a raise by an order of magnitude of the muon transfer rate to oxygen with energy from $E \sim 10$ meV to $E \sim 70$ meV, and confirm the efficiency of the FAMU method. In turn, the knowledge of detailed energy dependence $\lambda_{\mathrm{pO}}(E)$ provides a tool for modeling of the experiment and optimizing the experimental conditions for maximal efficiency. The results set a reliable benchmark for computations of charge exchange and other low energy inelastic processes with exotic atoms.

Acknowledgements The authors acknowledge the support of FNI Grant KP-06-N58/5.

References

[1] R. Pohl, A. Antognini, F. Nez, et al., *The size of the proton*, Nature 466, 213-216 (2010).

[2] Masaki Hori *et al. Laser spectroscopy of pionic helium atoms*, Nature 581, 37–41 (2020).

[3] The ALPHA Collaboration, *Investigation of the fine structure of antihydrogen*, Nature, 578, 375–380 (2020).

[4] A. Adamczak, D. Bakalov, K. Bakalova, E. Polacco, and C. Rizzo, *On the use of a H2-O2 gas target in muonic hydrogen atom hyperfine splitting experiments*, Hyperfine Interact. 136, 1 (2001).

[5] R. Pohl *et al.*, *Laser spectroscopy of muonic deuterium*. Science. 353 (6300): 669–673 (2016).

[6] A. Beyer et al., *The Rydberg constant and proton size from atomic hydrogen*, Science. 358 (6359): 79–85 (2017).

[7] N. Bezginov et al., *A measurement of the atomic hydrogen Lamb shift and the proton charge radius*, Science, 365 (6457): 1007–1012 (2019).

[8] A. Adamczak, D. Bakalov, L. Stoychev, and A. Vacchi, *Hyperfine spectroscopy of muonic hydrogen and the PSI lamb shift experiment*, Nucl. Instrum. Meth. B 281, 72 (2012).

[9] A. Werthmüller *et al.*, *Energy dependence of the charge exchange reaction from muonic hydrogen to oxygen*, Hyperfine Interactions 116, 1 (1998).

[10] A. Dupays, B. Lepetit, A. Beswick, C. Rizzo, and D. Bakalov, *Nonzero total-angular-momentum three-body dynamics using hyperspherical elliptic coordinates: Application to muon transfer from muonic hydrogen to atomic oxygen and neon*, Phys. Rev. A 69, 062501 (2004).

[11] Anh-Thu Le and C.D. Lin, *Muon transfer from muonic hydrogen to atomic oxygen and nitrogen*, Phys. Rev. A 71, 022507 (2005).

[12] Pizzolotto, A. Sbrizzi, A. Adamczak, et al.,*Measurement of the muon transfer rate from muonic hydrogen to oxygen in the range 70-336 K*, Phys. Lett. A 403, 127401 (2021).